

Review

# New Organic Materials Based on Multitask 2*H*-benzo[*d*]1,2,3-triazole Moiety

Iván Torres-Moya \* , José Ramón Carrillo, Ángel Díaz-Ortiz and Pilar Prieto 

Department of Inorganic, Organic Chemistry and Biochemistry, Faculty of Science and Chemical Technologies, University of Castilla-La Mancha, 13071 Ciudad Real, Spain; Joseamon.carrillo@uclm.es (J.R.C.); Angel.Diaz@uclm.es (Á.D.-O.); MariaPilar.Prieto@uclm.es (P.P.)

\* Correspondence: Ivan.TorresMoya@uclm.es

**Abstract:** Multifunctionality is a desirable aspect in materials science. Indeed, the development of multifunctional compounds is crucial for sustainable chemistry by saving resources and time. In this sense, 2*H*-benzo[*d*]1,2,3-triazole (BTz) is an excellent candidate with promising characteristics, including its ability to self-assemble; its acceptor character, which enables the synthesis of donor-acceptor structures; and its facile modulation using standard chemical methods. Thus, due to its interesting properties, it is possible to produce different derivatives with applications in different fields, as summarized in this article, with the correct substitution at the BTz cores. Optoelectronic or biomedical applications, amongst others, are highlighted.

**Keywords:** benzotriazole; optical waveguide; OFETs; TPA; organogels; biomarkers



**Citation:** Torres-Moya, I.; Carrillo, J.R.; Díaz-Ortiz, Á.; Prieto, P. New Organic Materials Based on Multitask 2*H*-benzo[*d*]1,2,3-triazole Moiety. *Chemosensors* **2021**, *9*, 267. <https://doi.org/10.3390/chemosensors9090267>

Academic Editor: Atanu Jana

Received: 16 August 2021

Accepted: 15 September 2021

Published: 17 September 2021

**Publisher's Note:** MDPI stays neutral with regard to jurisdictional claims in published maps and institutional affiliations.



**Copyright:** © 2021 by the authors. Licensee MDPI, Basel, Switzerland. This article is an open access article distributed under the terms and conditions of the Creative Commons Attribution (CC BY) license (<https://creativecommons.org/licenses/by/4.0/>).

## 1. Introduction

Today, technological development requires the use of more sophisticated, complex and high-performance devices and technologies. This evolution would not have been possible without the parallel development of new materials with improved performance, among which organic compounds have played a very prominent role. However, over the past few decades, there has been a marked growth in the use of organic materials as a promising alternative to their inorganic counterparts [1]. Despite the fact that, in general, these materials offer poorer performances than inorganic ones, they nevertheless exhibit excellent properties that make them promising candidates for the near future, especially their greater flexibility (due to their plastic mechanical properties), better processability (it is possible to work with these materials in solution), reduced working costs, and better adaptability to the required properties as they are easier to modify than inorganic materials. Furthermore, it is possible to work with small quantities of material due to their excellent photophysical properties, especially their high rates of absorption and emission.

For the design of these new materials, organic chemistry offers an important advantage from a synthetic point of view. The ideal situation would be that cheap materials that can be applied in various fields simultaneously and can be obtained by way of simple procedures. This is known as multifunctionality and is an upcoming area of research in the field of materials science as it may form the basis of a much more sustainable future [2,3].

In an attempt to develop multifunctional organic materials, over the past few years, we have been working with the BTz moiety, a much less widely studied benzoazole than other analogues, such as 2,1,3-benzoxadiazole (BOD), 2,1,3-benzothiadiazole (BTD), and 2,1,3-benzoselendiazole (BSD), due to its interesting characteristics and its enormous potential.

BTz (Figure 1) is a moderate electron acceptor moiety because of its polarizable imine unit (C=N) [4–6], which can be easily modified with the introduction of different substituents upon arylation or alkylation at the 2-position, thereby modulating the electron-acceptor properties. Furthermore, the benzene ring is very reactive, hence it is possible to introduce different groups to modulate the chemical structure and, as a consequence, its

properties. In addition, its planar character and its marked ability to self-assemble make BTz a promising moiety in material sciences, with applications in different fields given the appropriate choice of substituents [7–10].

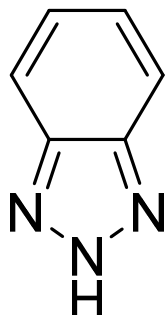


Figure 1. 2H-benzo[d][1,2,3-triazole (BTz).

As an electron-acceptor moiety, BTz has been widely used to build medium or wide band-gap donor-acceptor (D-A) systems, thus allowing intramolecular charge transfer (ICT) [11], and BTz can be used for that purpose. In addition, it has been reported that, among the benzazole derivatives containing different heteroatoms (N, O, S and Se), BTz exhibits the highest luminescence quantum yield [12].

It is noteworthy that BTz has found broad applications in industrial processes [13], in new technologies, and in everyday uses. Among them, it has been widely employed to build medium or wide band-gap D-A conjugated polymers for organic solar cells (OSCs) [14,15], or polymers with electroluminescent and electrochromic properties [16], and in the design of metal–organic frameworks (MOFs) [17]. In another sense, BTz is used as an anticorrosive agent in cooling, hydraulic, and antifreezing fluids [18]. Furthermore, BTz is used as a chemical intermediate in the synthesis of dyes, drugs, and fungicides. Finally, some BTz derivatives also have applications in biomedicine, so they can be considered to be a privileged structure given their various pharmacological activities, which explains why they have been used for the design of new pharmacologically active compounds [19] and have shown marked antiviral activity against many viruses [20,21].

All these excellent properties suggest the wide-ranging utility of the BTz unit. For these reasons, different modifications of the BTz moiety and their applications in different areas of material sciences are described herein, thus corroborating its multifunctional character and highlighting the versatility and enormous potential of the BTz core.

## 2. BTz as Optical Waveguides

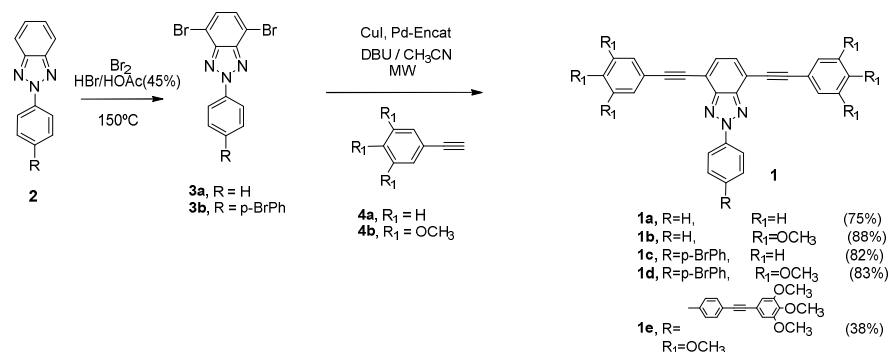
Nanophotonics is an emergent field of research [22,23] that aims to control and manipulate photons and optical energy on a nanoscale. This fact, together with the ability of photons to transport information, has opened the door to their application in optical technology. Their great potential may result in the development of new optical devices that overcome the fundamental limitations of bandwidth and power dissipation in silicon-based electronic circuits. The key components in these new photonic devices are the optical waveguides [24–26], which are the analogues of wires in electronic circuits.

Optical waveguides are physical structures that are able to absorb and transmit incident light. They possess a higher refractive index than their surroundings and allow the confinement of light according to the principles of Snell's law. Organic molecules with an ability to self-assemble have allowed production of the micro- or nanostructures with optical waveguiding behavior that are essential for such novel photonic devices.

We have experience with organic compounds with applications as optical waveguides. Thus, previous studies from our research group have shown the excellent behavior of 4H-1,2,4-triazole derivatives as optical waveguides [27,28]. For this reason, we proposed the synthesis of 2H-benzo[d][1,2,3-triazole derivatives (BTz), with the aim of studying the ability of these systems to self-assemble while varying their emissions, thus allowing us

to establish a structure–property relationship. The previously studied triazoles had a V shape, whereas BTzs adopt a T shape. In this regard, it is well known that optoelectronic properties are highly dependent on chemical structure and supramolecular aggregation.

The synthesis of arylolethynylbenzotriazoles (**1**) derivatives was performed according to the synthetic procedure described by Höger [29] (Scheme 1), with good yields, and all the synthetic procedures and experimental data are recorded in Supporting Information.



**Scheme 1.** Synthesis of 2*H*-benzo[*d*]1,2,3-triazole derivatives **1**.

The formation of organized supramolecular aggregates from compound **1** was achieved using the slow diffusion technique, with CHCl<sub>3</sub> as the good solvent and a variety of poor solvents, such as methanol, hexane, or acetonitrile. Only compounds **1b** and **1d**, with methoxy substituents, led to well-defined, needle-like aggregates, which were several hundred micrometers in length and around 10 μm in width. Benzotriazoles **1a** and **1c**, which lack of methoxy substituents, gave rise to amorphous solids, while compound **1e** did not lead to well-defined aggregates either, probably due to interdigitation of the methoxy groups.

The light propagation and optical waveguide behaviors of as-prepared aggregates of compounds **1b** and **1d** were studied. These studies were carried out using a confocal light microscope, irradiating the aggregates with a laser beam and collecting fluorescence images using a camera. Only the aggregates formed using benzotriazole **1b** showed properties of optical waveguides, with the incident light being conducted through the rod-like aggregates. Indeed, propagated light was observed at the ends of the **1b** aggregates when light was directed at the center of these aggregates. In contrast, the aggregate formed from compound **1d** did not show any optical waveguide behavior (Figure 2) [30].

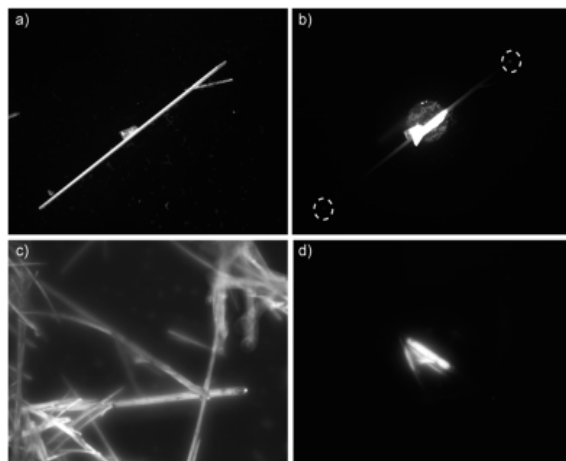
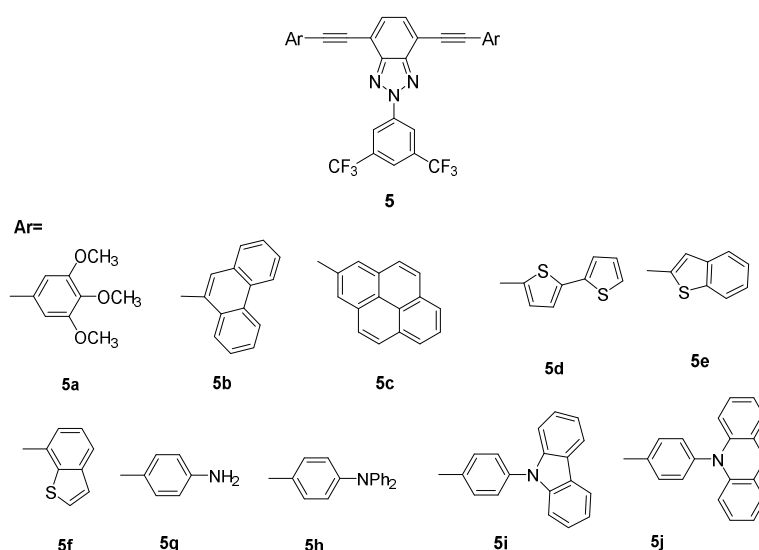


**Figure 2.** Polarized light (PL) microscopy images of the aggregates of **1b** (a,b) and **1d** (c,d), obtained by irradiating the entirety (left) or a portion (right) of the aggregate.

With this target in mind, the next purpose was to tune the luminescent properties of organic materials by modifying their chemical structure. Most 1D organic waveguides are made from  $\pi$ -conjugated small molecules with a structure that allows electron delocalization [31]. These  $\pi$ -conjugated systems can be modulated by incorporating different electron donor (D) and acceptor (A) moieties to facilitate intramolecular charge transfer (ICT) [32–39]. In this way, band-gap levels and optical properties can be easily tuned by modifying these donor and acceptor groups. Similarly, modification of the substituents in conjugated structures provides strong ICT, modulates the self-assembly behavior, facilitates crystal packing, and contributes to their photoluminescent properties. Furthermore, it is known that changes in the structure of molecular aggregates have a marked influence on their fluorescence properties, as well as wavelength [40,41].

Taking these considerations into account, the initial structure of the alkynyl benzotriazole derivatives was modified by introducing electron-withdrawing groups in the central ring and different alkynyl acceptor groups in positions 4 and 7 of BTz (Scheme 2). Trifluoromethylphenyl groups were chosen because of their known ability to self-assemble via C–F ... H–C and C–F ...  $\pi$  interactions [42–45]. Furthermore, aromatic donor groups with different geometries were chosen: planar, to favor aggregation via  $\pi$ – $\pi$  stacking, or voluminous and twisted, to decrease  $\pi$ – $\pi$  interactions and avoid the low fluorescence quantum efficiency mainly resulting from  $\pi$ – $\pi$  stacking of the planar backbones.

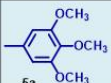
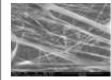
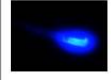


**Scheme 2.** Serie of D-A-D 2H-benzo[d]1,2,3-triazole derivatives 5.

In order to evaluate how substitution at the benzotriazole core of the donor substituents affected the optical waveguide behavior, aggregates of all compounds 5a–j were produced using the slow diffusion technique with various solvent mixtures.

After analyzing the SEM images of all the aggregates formed, only those with a single-crystal structure, smooth surfaces, and flat end facets (5a, 5b, 5e, 5f, 5i and 5j) were selected to study their optical waveguide behavior. Photoluminescence (PL) and SEM images of the aggregates studied are shown in Figure 3 [46].

The band-gap of the different structures were calculated computationally at B3LYP/6-31g(d,p) theory level and were in good agreement with the experimental ones calculated from the onset of the lowest energy absorptions in the UV-vis spectra. The results indicated a relationship between the band-gap and the color emission of the optical waveguide. Thus, compound 5a, which had a higher band-gap, exhibited blue light emission, whereas compounds with a lower band-gap (5b, 5e, 5f, 5i), exhibited green–red light emission, and 5j exhibited red emissions with a bathochromic shift due to having the lowest band-gap value. Thus, the goal of modulating the band gap of BTzs to obtain aggregates that behave as optical waveguides with different emission wavelengths has been achieved.

						
SEM Images						
Blue Waveguide						
Green Waveguide						
Red Waveguide						
Band gap (eV)	2.81	2.64	2.27	2.77	2.58	1.89

**Figure 3.** SEM images, images of fluorescence confocal microscopy, and DFT-calculated band-gap values for derivative 5.

Furthermore, it is well known that graphene has become a very promising material for new photonic and optoelectronic devices in the last few decades due to its interesting properties, such as its high carrier mobility and zero band-gap [47–49]. As such, in recent years, optical waveguides with embedded graphene have been studied because graphene can interact with localized photons in the waveguide [50–52].

In light of this, we doped BTzs with graphene with the aim of designing new optical waveguide structures with improved properties. Among the aggregates of synthesized BTzs 5, compound 5e showed very thick and well-defined fibers that acted as a waveguide for the colors green and red. The graphene used to form the aggregates was obtained by way of a solvent-free ball-milling process. [53–55] This low-layer (<4) powdered graphene (few-layer graphene, FLG) can be dispersed by sonication in polar solvents, which is essential for its interaction with BTz in the self-assembly process. This process was performed using the slow-diffusion technique, with tetrahydrofuran (THF) as a good solvent and CH<sub>3</sub>CN as a poor solvent. All processes were carried out with and without the addition of graphene. In both cases, well-defined needle aggregates were obtained (Figure 4), although bright spots were observed on the surface of the mixed aggregates (Figure 4-2c,d), thus indicating the presence of graphene.

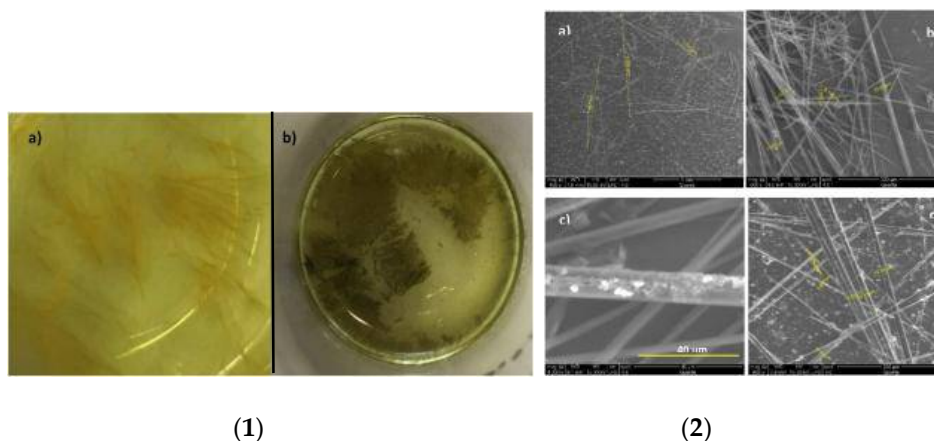


**Figure 4.** (1) Aggregates of compound 5e (a) and compound 5e + FLG (b) formed by the slow diffusion technique; (2) SEM images of the needles formed by the self-assembly of 5e (a,b) and 5e + FLG (c,d).

Raman spectroscopy confirmed the presence of FLG in the structure of the crystallized aggregates, because in Raman spectra, the  $C\equiv C$  vibration referred to BTz derivative **5e** and 2D band of graphene could be observed, corroborating the existence in the hybrid aggregate of BTz **5e** and graphene. Moreover, a deep profile analysis at different points of the aggregate indicated that the FLG was only deposited in the surface.

The role that graphene plays in the optical waveguide behavior of the aggregates was evaluated by observing the propagation of light in aggregates of **5e** with or without FLG.

The needles formed as a result of the self-assembly of compound **5e** transmitted green and red light, while the aggregates formed in the presence of FLG only transmitted green light (Figure 5) [56].

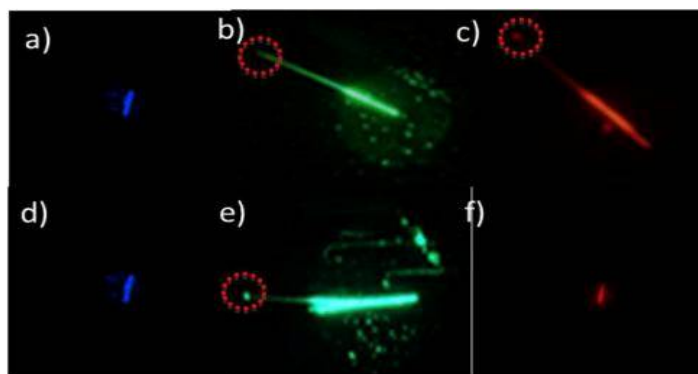


**Figure 5.** PL microscopy images of the needle-like aggregates of BTz derivative **5e** (a–c) and BTz derivative **5e** + FLG (d–f).

The graphene attached to the surface of BTz aggregates behaves like a cut-off filter, thus allowing more selective behavior of the aggregate as an optical waveguide. These results could be explained by considering that graphene induces a different energetic overlap between light and the aggregate. Perhaps, the different intermolecular interactions existing in the hybrid aggregate as compared to the pristine BTz aggregate could induce the absorption of the lower energy (red light) and do not absorb the high energy (green light) which is emitted.

In summary, a more selective waveguide has been achieved by doping the chemical structure, a methodology that could be of great interest in photonic devices.

### 3. BTz as Semiconductor in Organic Field-Effect Transistors (OFETs)

Organic molecules have attracted research interest over the past few years due to their enormous potential as semiconductors in electronic devices like organic field-effect transistors (OFETs) [57,58]. These kinds of devices basically consist of a dielectric layer, an organic semiconductor layer, and three electrodes (gate, source, and drain), and are the key for the upcoming generations of low-cost and flexible organic circuits.

A wide range of organic molecules have been commonly used as organic semiconductors in OFETs, including donor-acceptor (D-A) derivatives, thus allowing the intramolecular charge transfer [11], which is a valuable property for this kind of device.

In that sense, the D-A-D-based BTz system **5** previously described in Scheme 2 could provide an interesting architecture for use as the organic semiconductor layer in order to fabricate electronic devices.

The electrical properties of the D-A-D-based BTz derivatives **5** and their possible implementation as organic semiconductors in OFETs were tested by the fabrication of OFETs with a top-contact/bottom-gate field-effect transistor architecture through organic semiconductor vapor deposition by sublimation technique, in vacuum conditions, on substrates of Si/SiO<sub>2</sub> previously treated with hexamethyldisilazane (HMDS) or octadecyltrichlorosilane (OTS). The process continued through the thermal gold deposition, employing shadow masks in order to define the electrode's source and drain. The parameters that determine the efficiency of an OFET were extracted from the I-V plots, working with the saturation regime in Equation (1), and these were field-effect mobility ( $\mu$ ), ratio  $I_{ON}/I_{OFF}$ , and threshold voltage ( $V_T$ ) [59,60]

$$(I_D)_{\text{sat}} = (W/2L)\mu C(V_G - V_T)^2 \quad (1)$$

In this equation,  $W$  is the width of the channel,  $L$  the length of the channel,  $C$  the capacitance per unit area or the insulator layer, and  $V_G$  is the voltage applied in the gate.

The results of the parameters calculated for films of **5** using Equation (1) can be found in Table 1.

**Table 1.** OFET electrical data for devices fabricated with organic semiconductors **5** measured in vacuum.

Semiconductor (HMDS 90 °C)	HOMO * (eV)	LUMO * (eV)	$\mu_h$ (cm <sup>2</sup> V <sup>-1</sup> s <sup>-1</sup> )	$V_T$ (V)	$I_{ON}/I_{OFF}$
<b>5b</b>	−5.29	−2.65	$2.69 \times 10^{-4}$	−57	$2 \times 10^3$
<b>5c</b>	−5.07	−2.68	$3.31 \times 10^{-5}$	−40	$1 \times 10^2$
<b>5e</b>	−5.10	−2.83	$1.80 \times 10^{-4}$	−69	$8 \times 10^3$
<b>5f</b>	−5.41	−2.64	$3.76 \times 10^{-5}$	−13	$4 \times 10^2$
<b>5h</b>	−4.81	−2.42	$1.21 \times 10^{-4}$	−38	$2 \times 10^2$
<b>5i</b>	−5.30	−2.72	$2.02 \times 10^{-5}$	−58	$3 \times 10^2$
<b>5j</b>	−4.73	−2.84	$2.04 \times 10^{-4}$	−40	$5 \times 10^2$

\* HOMO and LUMO has been theoretically calculated at B3LYP/6-31g(d,p) theory level.

These results show that seven compounds exhibited hole-transport ability, thus indicating their behavior as p-type semiconductors [61]. These findings are in agreement with the values for the HOMO and LUMO frontier orbitals, calculated at the B3LYP/6-31g(d,p) level of theory. All the HOMO values for these derivatives **5** were about −5.0 eV, near the Fermi level for gold, which is the working electrode employed in these devices. However, the LUMO levels were far from the Fermi level for gold, thus hindering electron transport between this level and the LUMO, which could explain why these derivatives acted as p-type rather than n-type semiconductors.

The hole mobilities ( $\lambda_h$ ) were around  $10^{-4}$  to  $10^{-5}$  cm<sup>2</sup>V<sup>-1</sup>s<sup>-1</sup> in all cases. We observed that there was a relationship between the mobilities and the degree of  $\pi$ -conjugation obtained by Raman spectroscopy, focusing our attention on the C≡C stretching frequencies (Table 2). In general, a lower ring aromaticity leads to enhanced charge delocalization across the structure, thereby improving the behavior as organic semiconductor in OFETs. As a consequence, the charges injected into the device via the gate will be better stabilized in less-aromatic compounds. For this reason, compound **5e**, which exhibited a lower  $\nu(\text{C}\equiv\text{C})$  frequency, was a better semiconductor than **5f**, because thiophene was less aromatic than benzene and allowed a better charge delocalization in the structure, thus improving the semiconductor character. In this sense, **5b** and **5c** showed similar behaviors and a similar explanation can be applied to these derivatives.

This study demonstrated the applicability of BTz derivatives **5** in organic electronics as organic semiconductors in OFETs. Moreover, due to the high versatility of this moiety, possible future modifications of these derivatives could improve their mobility and applicability as n-type semiconductors or ambipolar systems.

**Table 2.** Values of the vibrations object of studied by Raman spectroscopy for semiconductors 5. Theoretical values obtained at B3LYP/6-31g(d,p) level appear in brackets.

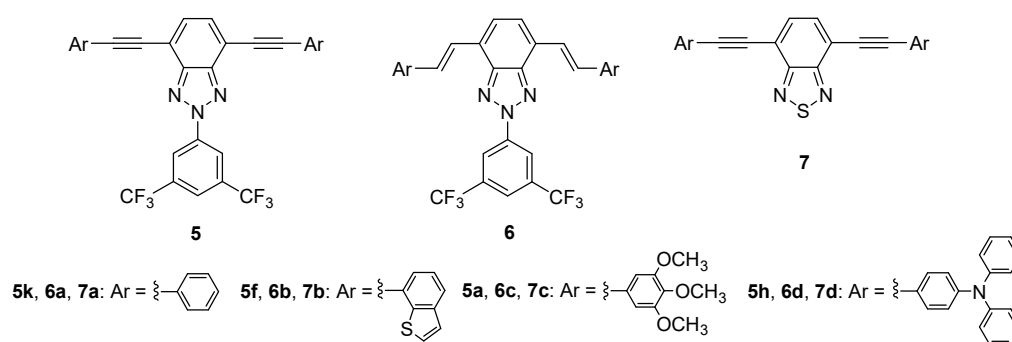
Compound	Benzotriazole Band (cm <sup>-1</sup> )	C≡C Triple Bond Stretching (cm <sup>-1</sup> )
5a	1474 (1462)	2202 (2300)
5b	1474 (1460)	2197 (2287)
5c	1476 (1460)	2207 (2277)
5d	1473 (1459)	2187 (2272)
5e	1472 (1456)	2193 (2259)
5f	1472 (1461)	2200 (2295)
5g	1472 (1461)	2204 (2291)
5h	1473 (1461)	2198 (2289)
5i	1475 (1461)	2193 (2296)
5j	1474 (1461)	2210 (2300)

#### 4. BTz as Two Photon Absorption (TPA)

TPA spectroscopy has been promoted as a useful tool for studying the general properties of materials and interactions between matter and light. In recent years, materials displaying TPA have gained attention for the development of attractive applications like 2D microfabrication [62], optical data storage [63], and two-photon induced fluorescence (TPIF) imaging [64].

The most promising TPA properties have been observed in quadrupolar  $\pi$ -conjugated structures with terminal donor or acceptor substituents, and with symmetrical designs bearing peripheral donor groups, e.g., D- $\pi$ -D or D- $\pi$ -A- $\pi$ -D systems [65–70]. Moreover, ICT is an essential requirement for high TPA cross-sections, which is the crucial parameter for evaluating TPA capacity.

Despite the fact that the 1,2,5-benzothiadiazole (BTD) moiety has been employed as an electron-withdrawing core in molecules with TPA properties [71–73], to the best of our knowledge the BTz unit has not been employed in this aspect. In this regard, and with the idea in mind of gaining a more in-depth understanding of the relationship between structure and TPA properties, we studied three different conjugated benzoazole derivative families, including several alkynyl derivatives of BTz (5), alkenyl-BTz derivatives (6), and BTD derivatives (7) (Figure 6).

**Figure 6.** Series of benzoazoles studied in TPA conditions.

Compounds 5 and 7 were prepared by means of a Sonogashira C-C cross-coupling reaction under microwave irradiation from the dibromobenzoazole 3 and the corresponding arylalkynyl derivative [46,61,74,75]. Alkenyl benzoazoles 6 were obtained through a Heck C-C cross-coupling reaction between the dibromobenzoazole 8 and the corresponding arylalkene (compounds 6a,c,d, 41–86%) or upon partial reduction of 5f (in the case of 6b, 71%) [76]. The synthetic procedure and experimental data of these compounds can be found in Supporting Information.

Working under one-photon conditions (OP), the absorption spectra showed the longest wavelength bands between  $\lambda = 373$  and 490 nm, which were associated with S1←S0

transitions. Greater conjugation in the compound, which is favored by the presence of a vinylene instead of an acetylene bridge, promotes electronic movement and the red-shifting of these bands. The fluorescence bands of compounds **5–7** localized around a large spectra region ( $\lambda = 450\text{--}625\text{ nm}$ ), exhibiting Stokes shifts of up to  $6415\text{ cm}^{-1}$ . These dyes showed moderate to high fluorescence quantum yields ( $\varphi_{\text{fluor}} = 0.20\text{--}0.78$ ). The lower values of the compounds **6a–d** were a consequence of the photoisomerization processes.

The TPA properties of these derivatives were studied by TPIF from  $\lambda = 700$  to  $1000\text{ nm}$  (Table 3). The results showed that the chromophores with the stronger electron-donor substituent, namely triphenylamino, had the highest cross-section values:  $1510\text{ GM}$  at  $840\text{ nm}$  for **5h**,  $790\text{ GM}$  at  $830\text{ nm}$  for **6d**, and  $545\text{ GM}$  at  $830\text{ nm}$  for **7d** (Figure 7). Compounds bearing a  $\text{C}=\text{C}$   $\pi$ -bridge (**6a–d**) had a higher conjugation than those bearing a  $\text{C}\equiv\text{C}$   $\pi$ -bridge (**5**) and better TPA properties. The higher cross-section value of **5h** in comparison with **6d** can be explained by taking into account the movement of the electrons and the steric congestion. Finally, dyes bearing a BTz core exhibited similar or better cross-sections than the BTd counterparts. The presence of the 3,5-bis(trifluoromethyl)phenyl group increased the electron-withdrawing character of the BTz dyes under TP conditions. Additionally, these derivatives showed notable brightness values of up to  $483\text{ GM}$ .

**Table 3.** TPA cross sections of compounds **5–7** measured in the range of  $\lambda = 700\text{--}1000\text{ nm}$ .

Compound	$\sigma[\text{GM}]$	Compound	$\sigma[\text{GM}]$	Compound	$\sigma[\text{GM}]$
<b>5k</b>	9	<b>6a</b>	39	<b>7a</b>	29
<b>5f</b>	33	<b>6b</b>	125	<b>7b</b>	129
<b>5a</b>	104	<b>6c</b>	131	<b>7c</b>	88
<b>5h</b>	1510	<b>6d</b>	790	<b>7d</b>	545

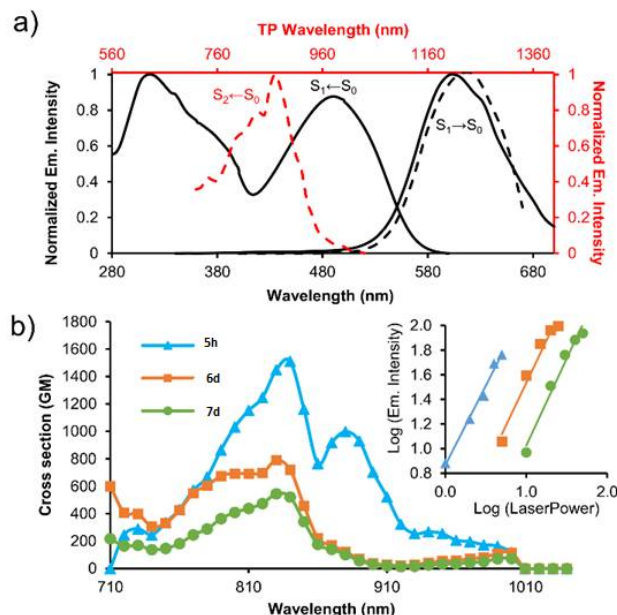


**Figure 7.** (a) Absorption and emission spectra of **6d** under the OP regime (bold lines). Excitation (red dashed line) and emission spectra (black dashed line) of **6d** under TP conditions. The electronic states involved are indicated in each case; (b) Cross-sections of compounds **5h** (triangles), **6d** (squares), and **7d** (circles). The inset shows the double-logarithmic plot of the emission maximum intensity vs. laser power for these compounds.

DFT calculations were performed for all compounds mentioned. A natural transition orbital (NTO) analysis for the transitions with the lowest energy ( $\text{S1}\leftarrow\text{S0}$ ) showed that the NTO holes were centered on the donor groups and the  $\pi$ -bridge. In contrast, NTO electrons

were fully localized along the core of the molecules. This fact is related to an ICT process, in agreement with the experimental data.

The TPA properties were evaluated at the CAM-B3LYP/6-31G theory level. All the theoretical data showed that the active transition under TP conditions was  $S_2 \leftarrow S_0$ . NTO analysis for the later transition corroborated that the properties as a TP chromophore were closely related to the change in the electron density distribution. As an example, the  $S_2 \leftarrow S_0$  transitions for the compounds that exhibited the lowest and highest experimental cross-section values, **5k** and **5h**, respectively, are indicated in Figure 8. In dye **5k** the electron density was located on the acceptor core, where, independently, we considered the NTO hole or NTO electron. However, in dye **5h**, the electron density dramatically moved from the donor groups in the NTO hole to the acceptor unit in the NTO electron.

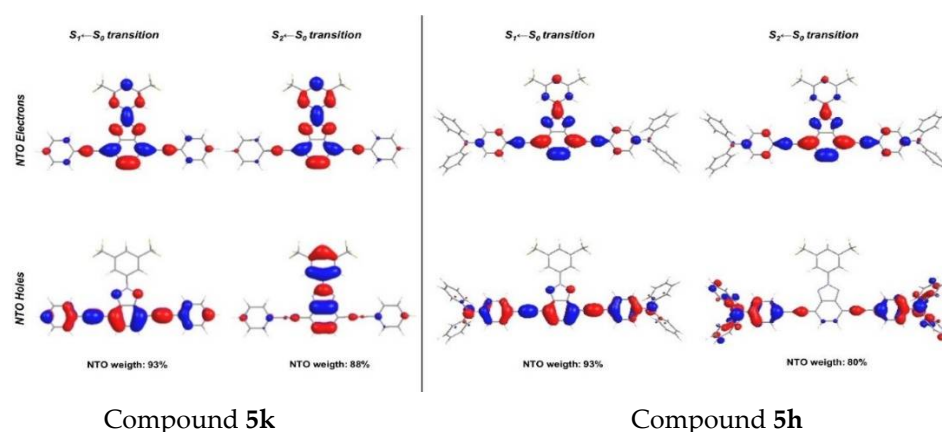


Figure 8. NTOs for  $S_1 \leftarrow S_0$  and  $S_2 \leftarrow S_0$  transitions in compounds **5k** and **5h**.

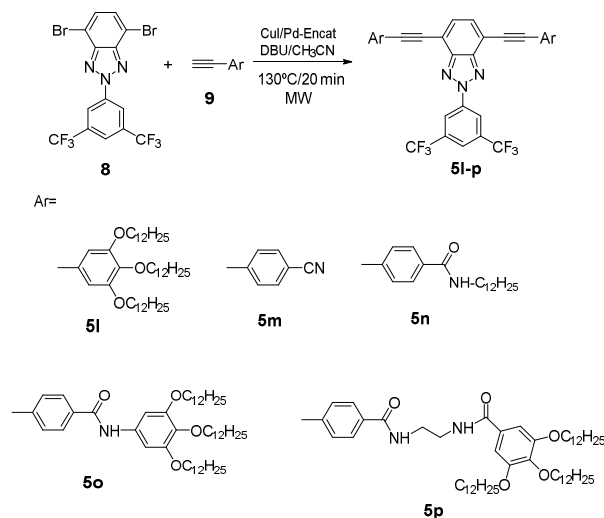
## 5. BTz as Organogels

Organogels are characterized by their continuous organic phase and can be further subdivided based on the nature of the gelator molecule as polymers or low-molecular-weight (LMW) organogelators. The latter generally form gels due to the presence of self-assembled fibers via hydrogen bonds, van der Waals forces, and  $\pi$ -stacking.

In this context, and with the aim of extending the applicability of 2*H*-benzo[*d*]1,2,3-triazole derivatives, promising gelators were synthesized via a C-C Sonogashira coupling reaction between the dibromobenzotriazole derivative (**8**) and different alkynyl fragments (**9**) (Scheme 3). It is well known that long chains [77] or amide groups [78], which can provide flexibility and allow hydrogen bonding, are promising functionalities in compounds to achieve gels. In addition, it has been also reported in the literature that the presence of a cyano group could allow the formation of promising gelators [79,80]. Hence, with this in mind, five different alkynyl derivatives with different promising functionalities were synthesized using the procedure described above. All the information about synthetic procedure and experimental data can be found in Supporting Information.

Once compounds **5l–p** were characterized, their gel behavior was studied by performing gelation tests. Thus, they were dissolved in thirty different solvents, and at different concentrations (2 wt %, 1 wt %, and 0.5 wt %). The vials were then sonicated for 30 s until complete dissolution. Finally, the vials were heated and kept undisturbed while cooling until room temperature, then the inversion tube test was used to check the gelation behavior.

The CN derivative, **5m**, did not form gels in any solvent, whereas **5l** gave gels in four solvents (1-pentanol, 2-propanol, methanol, and 1,4-butanediol) at a concentration of 2 wt %. At lower concentrations, **5l** lost its gel properties, as is usual. The gelator **5n** gave only one gel in 1,4-butanediol and **5o** gave gels in DMF and diethylene glycol at a concentration of 2 wt %.



**Scheme 3.** Synthesis of the promising gelators **5l–p** derived from BTz.

Compound **5p** showed the best tendency to form gels due to its enhanced ability to undergo supramolecular interactions. In this case, at a concentration of 2 wt %, this compound gave gels in different solvents (DMF, ethanol, methanol, 1-butanol, and 1-propanol) and partial gels in benzyl alcohol, 2-butanol, 2-propanol, and 1,4-butanediol. In this case, the gel behavior even increased with a decrease in concentration from 2 to 1 wt %. In this case, gels were formed in ethanol, methanol, hexane, 2-butanol, 1-propanol, 1-butanol, 2-propanol, and 1,4-butanediol, and partial gels were formed in benzyl alcohol and DMF. Finally, it should be noted that gels were even achieved at a low concentration of 0.5% in ethanol, 1-butanol, 1-propanol, 2-butanol, 2-propanol, and 1,4-butanediol (Figure 9).

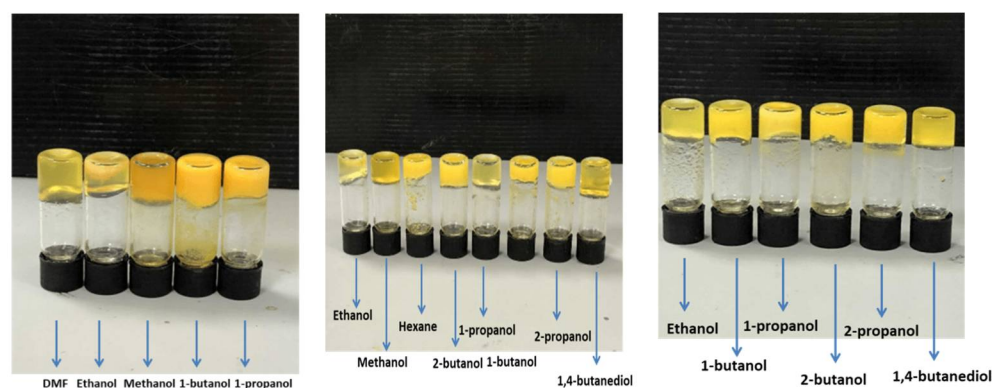


**Figure 9.** Gels for **5p** at concentrations of 2% wt (left), 1% wt (center) and 0.5% wt (right).

The CGCs (critical gelation concentration, the minimal amount of compound that is needed to obtain a gel) for **5p** was very low, thus corroborating the high tendency to form gels. In ethanol, this gelator gave gels at a concentration of only 0.1 wt % (Figure 10) and can therefore be considered to be a “supergelator” [81,82], probably due to the strong aggregation between alcohol and amide groups via hydrogen bonds, an effect that has been described previously for tris(amide) derivatives [83].

The  $T_{sol}$  values (gel-to-sol phase transition temperature) for **5p** were particularly remarkable, being very high irrespective of concentration. It is noteworthy that it is very difficult to find gels as stable as these. The strong hydrogen bonds between the protons in the N-H groups and interdigitation between the long alkyl chains may explain the strength of these gels and the high  $T_{sol}$  values.

Rheology stress experiments were performed to verify the strength of the organogels. The yield stress ( $\sigma$ ) was calculated at the point where the gels broke down [84]. In general,

high values of yield stress indicate a higher stability of the gel. Gels of **5p** proved to be particularly robust, exhibiting  $\sigma$  values of more than 1000 Pa in 1,4-butanediol and 1-butanol.

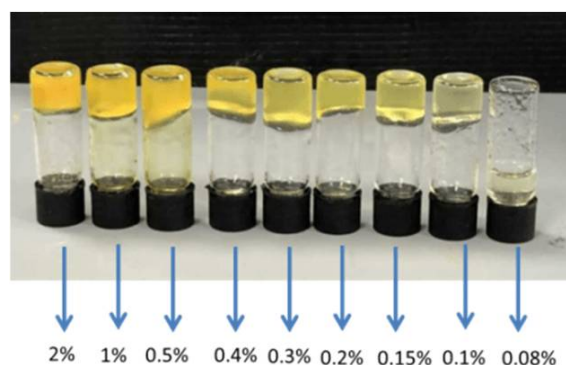


**Figure 10.** Gels for **5p** in ethanol at different concentrations (wt %).

The excellent properties of **5p** gels, especially their low CGC, high  $T_{sol}$ , and high yield stress in rheology experiments, highlight the robustness and stability of the gels and these facts support the potential application of these organogelators in drug delivery systems or for drug crystallization. However, as they may be toxic for humans, given the use of organic solvents, drug crystallization applications were chosen and organogels of **5p** were used as potential crystallization media for active pharmaceutical ingredients (APIs).

A diverse selection of different APIs (theophylline, sulfathiazole, sulfamerazine, and niflumic acid) were chosen based on their well-known polymorphism. For drug crystallization inside organogels of **5p**, previously optimized gelation conditions of a 10 mg/mL drug concentration at a concentration of 0.1% of gelator were used. A mixture of the gelator and the different drugs in a specific solvent was heated, followed by sonication to give a gel of the API solution. The vials were then left undisturbed at room temperature to allow crystallization, which can take several weeks. The vials in which crystals were observed were analyzed by X-ray powder and single-crystal diffraction.

In the cases of theophylline, sulfamerazine, and niflumic acid, no significant differences between solution crystallization and the crystallization inside the gel were observed. Our findings showed that Form II was obtained in both cases of theophylline in ethanol [85,86], the Pna21 polymorph in the case of sulfamerazine [87], and P21/n form in the case of niflumic acid.

For theophylline and sulfathiazole, slightly larger needle-shaped crystals were obtained by gel crystallization in comparison with solution crystallization. In the case of niflumic acid, a change in crystal pattern was observed. Thus, block-shaped crystals were obtained inside the gels in methanol, compared with needle forms obtained upon solution crystallization.

The case of sulfathiazole, in which a change in polymorphism from polymorphic Form II after solution crystallization to kinetic Form I [88,89] inside the gel was observed, should be highlighted (Figure 11). This interesting outcome suggests that the **5p** gelator either inhibits crystallization of Form II or increases the nucleation rate of Form I. These findings may be crucial for the pharmaceutical industry, thus opening the door to new applications of this drug [90].

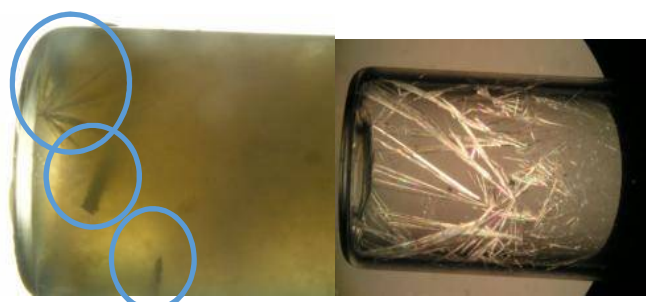


**Figure 11.** Crystals of sulfathiazole grown in 1-propanol gels of **5p** (left) and by solution evaporation (right).

## 6. BTz as Biomarker

Finally, biomarkers have become powerful tools in biology and biotechnology research since they can provide information on specific biological or molecular processes because of the labelling and imaging of biological systems that are not fluorescent [91,92]. In general, biomarkers should show different desirable characteristics, such as a high extinction coefficient and fluorescent quantum yield, high affinity for the biological target of interest, high water solubility, and photostability, and should also exhibit good biocompatibility and be easily adaptable to different experimental conditions. Moreover, they should not be affected by changes in different parameters, like ionic strength, pH, or temperature [93].

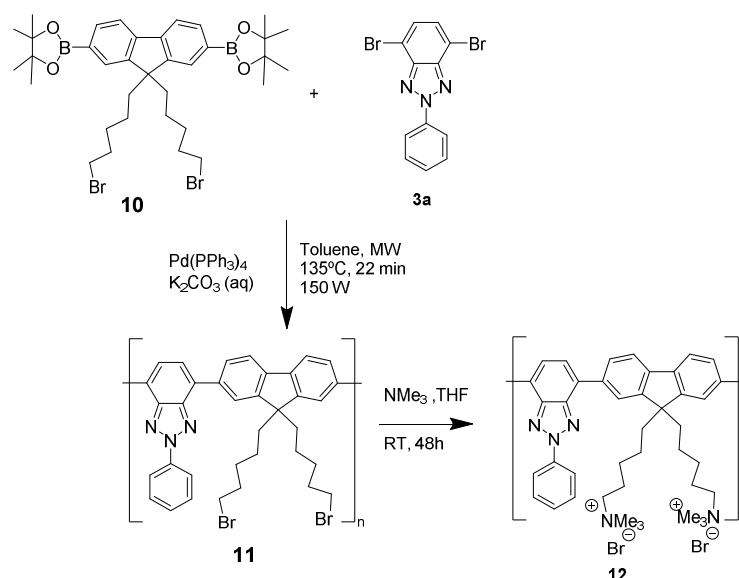
Conjugated polyelectrolytes (CPEs) with alkyl fluorene derivatives are very interesting in regards to the synthesis of potential biomarkers because of their interesting characteristics, especially their excellent chemical and thermal stability, photostability, high fluorescence efficiency, and good synthetic tunability due to the ease of substitution at C9 of the fluorene unit. Blue emission is the most usual in fluorene-based CPEs, whereas copolymerization with other aromatic units leads to a bathochromic shift [94–97]. As such, CPEs have been successfully employed as both blue and red biomarkers [98–101].

The use of green fluorescent biomarkers, a priori, seems to be less interesting due to the short penetration distance of these wavelengths in tissue. However, in the moment when the surface is being photographed, green biomarkers possess remarkable advantages instead of red ones due to their higher fluorescence emission efficiency and the ability to differentiate them from the auto-fluorescence of the background.

In this regard, given the photophysical properties of the BTz moiety, we focused on designing a green CPE with potential applications as a biomarker. Thus, we synthesized a CPE containing BTz and fluorene, as shown in Scheme 4 [98]. More details about synthetic procedure and experimental data can be found in Supporting Information.

The CPE copolymer **12** was successfully synthesized in good yield by way of a two-step reaction. The first step involved a microwave-assisted Suzuki cross-coupling reaction between dibromobenzotriazole **3a** and the diboronic derivative **10**, followed by quaternization (Menschutkin reaction). The as-prepared copolymer **11** exhibited a maximum peak at around 490 nm, with a large Stokes shift. These results indicate that an effective conjugation took place between 2-phenylbenzotriazole and fluorene, thus leading to the green emission band observed at 500 nm. Subsequent derivatization of **11** to obtain the polyelectrolyte **12** resulted in a slight red-shift in the absorption and emission maxima due to changes in the conformation of the polymer chains upon incorporation of the cationic groups.

Furthermore, different photostability studies and studies with different stimuli have supported its potential application as a biomarker. These aspects were explored using model membranes comprising anionic and zwitterionic lipids together with vesicles of phosphatidylglycerol (PG), which has a marked anionic character, and phosphatidylcholine (PC), which is zwitterionic in nature.



**Scheme 4.** Synthesis of copolymer **12**.

The calculation of the partition coefficient in PG and PC vesicles showed the higher affinity of the copolymer **12** for anionic vesicles. These results suggest the potential use of **12** to specifically target anionic lipid head groups. With the idea in mind of checking this hypothesis, vesicles doped with **12** were first explored by phase-contrast and fluorescence microscopy.

Figure 12 shows images of PG vesicles recorded before and after addition of the CPE **12**. Without the presence of **12** (Figure 12A), vesicles were observed by phase-contrast microscopy and upon irradiating the samples with visible light, no fluorescence was registered. On the other hand, when the CPE **12** was added to the same sample, green fluorescence could clearly be visualized under visible light illumination (Figure 12B). Similar results were obtained when employing PC rather than PG vesicles. In addition, it can be seen that the morphology and size of the PG and PC vesicles remained the same before and after addition of the CPE, which is crucial for their application as biomarkers.

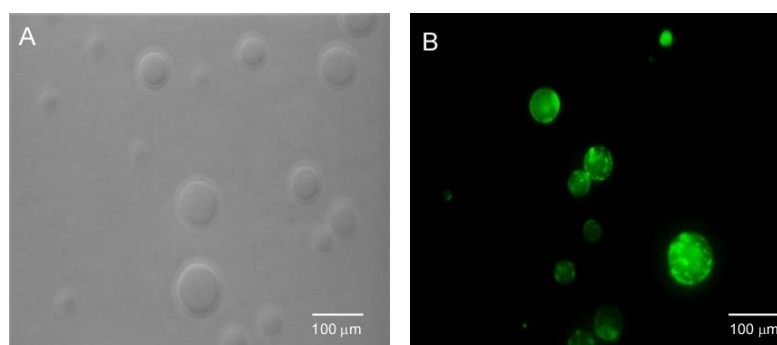


**Figure 12.** (A). Phase-contrast image of PG vesicles in the absence of CPE **12**; (B) Fluorescence microscopy image detected after the addition of the polyelectrolyte to the previous sample in a different field, recorded upon excitation with Vis-light using the FITR filter set.

After the ability of the polyelectrolyte to image membrane structures had been confirmed, a comparative study was performed with two series of vesicles containing anionic (PG) or zwitterionic phospholipids (PC). The zwitterionic PC was marked with the fluorescent probe BODIPY 581/591 C11. The same volumes of both samples were placed on a well slide and microscopy images were recorded before and after CPE addition (Figure 13). As we might have expected, both types were observed in phase contrast in the absence of

polyelectrolyte (Figure 13A), but the fluorescence of only some of them (the marked PC vesicles) was visualized upon excitation with the DsRed filter set (Figure 13B).

In Figure 14, the fluorescence microscopy images of the same field and obtained after the addition of CPE and upon excitation using either the FITR filter set (Figure 14B) or the DsRed filter set are shown (Figure 14C) (Figure 14A refers to the image in the visible light field). These images show that the vesicles exhibiting green fluorescence were different from those exhibiting red fluorescence. This result clearly shows that CPE selectively labelled the anionic vesicles. The bacterial membrane was rich in phospholipids with anionic head groups, hence this fact makes CPE an appropriate candidate for detecting bacterial cells by selectively targeting the bacterial membrane rather than mammalian cells, most of which have a zwitterionic membrane surface [102].

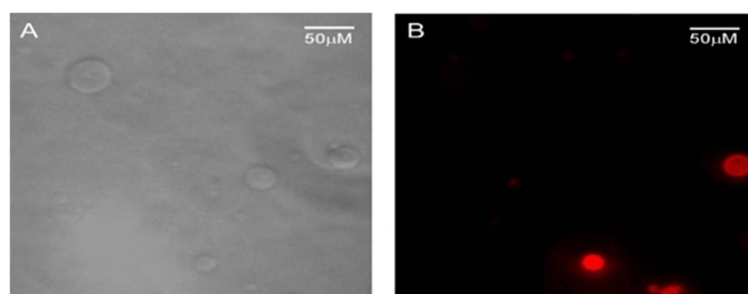


**Figure 13.** Microscopy images of PG vesicles in a mixture with PC-BODIPY vesicles obtained with (A) phase contrast and (B) upon excitation with Vis-light using the Leica DsRed filter. (A,B) images are from the same field.

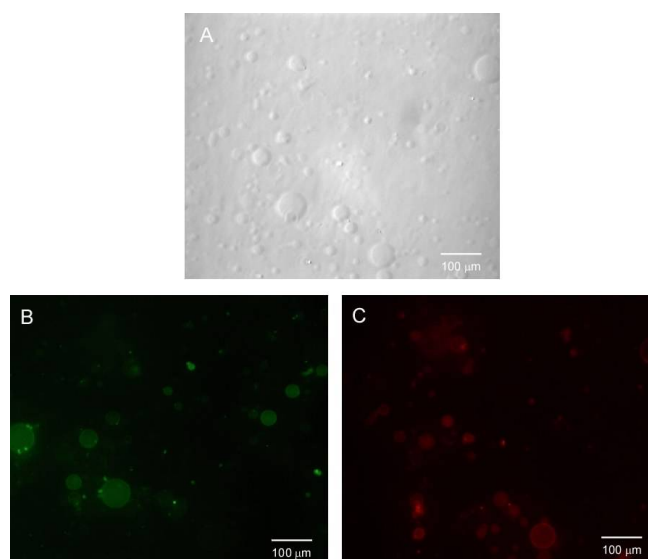


**Figure 14.** Fluorescence microscopy images of a mixture of PG and PC-BODIPY vesicles obtained after CPE addition, upon excitation with Vis-light (A), using the FITR filter set (B) and the DsRed filter set (C). All images correspond to the same field.

## 7. Conclusions

The research performed by our research group over the past few years, as discussed herein, shows the multifunctional nature of 2*H*-benzo[*d*]1,2,3-triazole derivatives. Their interesting properties and ready tunability make them an interesting multifunctional moiety in material sciences. Moreover, it has been demonstrated that, with the appropriate substitution, it is possible to synthesize organic compounds with applications in different fields, such as optical waveguides, organic field-effect transistors, TPA, organogels, and polymers in biomedicine.

The good modulation capacity of the BTz moiety and the high versatility thereof highlighted in this paper opens the door to new modifications for new applications or to improve their properties in the fields discussed in this article.

**Supplementary Materials:** The following are available online at <https://www.mdpi.com/article/10.3390/chemosensors9090267/s1>, The synthesis procedures and all the experimental data recorded in this article are available in Supporting Information.

**Author Contributions:** I.T.-M. synthesized all the compounds and performed all the studies reported. Furthermore, he took part in the writing draft elaboration and the work organization. J.R.C. helped with the interpretation of the results and also wrote part of the manuscript, Á.D.-O. helped with the interpretation of the synthetic results and also wrote part of the manuscript. P.P. planned and coordinated the work of the different groups and supervised and also wrote part of the manuscript. All authors have read and agreed to the published version of the manuscript.

**Funding:** This research was funded by JCCM-FEDER (project SBPLY/17/180501/000189) and MICINN (project PID2020-119636GB-I00 and RED2018-102331-T).

**Institutional Review Board Statement:** Not applicable.

**Informed Consent Statement:** Informed consent was obtained from all subjects involved in the study.

**Data Availability Statement:** The data collected in this review are available at references [30,46,61,76,90,102] described in this article. All of them are works reported by our research group.

**Acknowledgments:** I. Torres-Moya is indebted to the Junta de Comunidades de Castilla-La Mancha for a post-doctoral grant. The authors would like to thank Pablo Fernández for his assistance in the purification of the products and the work lab. Technical support from the High-Performance Computing Service of the University of Castilla-La Mancha is also acknowledged.

**Conflicts of Interest:** The authors declare no conflict of interest.

## References

1. Fraxedas, J. *Molecular Organic Materials. From Molecules to Crystalline Solid*; Cambridge University Press: New York, NY, USA, 2006.
2. Neena, K.K.; Sudhakar, P.; Dipak, K.; Thilagar, P. Diarylboryl-phenothiazine based multifunctional molecular siblings. *Chem. Commun.* **2017**, *53*, 3641–3644. [[CrossRef](#)]
3. Sinha, S.; Chowdhury, B.; Ghoraib, U.K.; Ghosh, P. Multitasking behaviour of a small organic compound: Solid state bright white-light emission, mechanochromism and ratiometric sensing of Al(III) and pyrophosphate. *Chem. Commun.* **2019**, *55*, 5127–5130. [[CrossRef](#)]
4. Tanimoto, A.; Yamamoto, T. Nickel-2,2'-Bipyridyl and Palladium-Triphenylphosphine Complex Promoted Synthesis of New  $\pi$ -Conjugated Poly(2-hexylbenzotriazole)s and Characterization of the Polymers. *Adv. Synth. Catal.* **2004**, *346*, 1818–1823. [[CrossRef](#)]
5. Balan, A.; Baran, D.; Toppare, L. Benzotriazole containing conjugated polymers for multipurpose organic electronic applications. *Polym. Chem.* **2011**, *2*, 1029–1043. [[CrossRef](#)]
6. Balan, A.; Gunbas, G.; Durmus, A.; Toppare, L. Donor–Acceptor Polymer with Benzotriazole Moiety: Enhancing the Electrochromic Properties of the Donor Unit. *Chem. Mater.* **2008**, *20*, 7510–7513. [[CrossRef](#)]
7. Patel, D.; Fude, F.; Ohnishi, Y.; Abboud, K.; Hirata, S.H.; Schanze, K.S.; Reynolds, J.R. It Takes More Than an Imine: The Role of the Central Atom on the Electron-Accepting Ability of Benzotriazole and Benzothiadiazole Oligomers. *J. Am. Chem. Soc.* **2012**, *134*, 2599–2612. [[CrossRef](#)] [[PubMed](#)]
8. Liu, B.; Ye, S.; Zou, Y.; Peng, B.; He, Y.; Zhou, H. A Dithienyl Benzotriazole-based Polyfluorene: Synthesis and Applications in Polymer Solar Cells and Red Light-Emitting Diodes. *Chem. Phys.* **2011**, *212*, 1489–1496. [[CrossRef](#)]
9. Dong, Y.; Cal, W.; Wang, M.; Li, Q.; Yilg, L.; Huang, F.; Cao, Y. [1,2,5]Thiadiazolo[3,4-f]benzotriazole based narrow band gap conjugated polymers with photocurrent response up to 1.1  $\mu$ m. *Org. Electron.* **2013**, *14*, 2459–2467. [[CrossRef](#)]
10. Dong, Y.; Cai, W.; Hu, X.; Zhong, C.; Huang, F.; Cao, Y. Synthesis of novel narrow-band-gap copolymers based on [1,2,5]thiadiazolo[3,4-f]benzotriazole and their application in bulk-heterojunction photovoltaic devices. *Polymers* **2012**, *53*, 1465–1471. [[CrossRef](#)]
11. Wu, Y.; Zhu, W. Organic sensitizers from D– $\pi$ –A to D–A– $\pi$ –A: Effect of the internal electron-withdrawing units on molecular absorption, energy levels and photovoltaic performances. *Chem. Soc. Rev.* **2013**, *42*, 2039–2058. [[CrossRef](#)]
12. Ghosh, S.; Pati, P.B.; Zade, S.S. Effect of the change of heteroatom on phenyl capped benzazole: Photophysical and electrochemical properties from the structural viewpoint. *J. Lumin.* **2018**, *194*, 164–169. [[CrossRef](#)]
13. Minella, M.; De Laurentiis, E.; Pellegrino, F.; Prozzi, M.; Dal Bello, F.; Maurin, V.; Minero, C. Photocatalytic Transformations of 1H-Benzotriazole and Benzotriazole Derivates. *Nanomaterials* **2020**, *10*, 1835. [[CrossRef](#)]

14. Zhang, Q.; Xiao, B.; Du, M.; Li, G.; Tang, A.; Zhou, E. A2–A1–D–A1–A2 type non-fullerene acceptors based on methoxy substituted benzotriazole with three different end-capped groups for P3HT-based organic solar cells. *J. Mater. Chem. C* **2018**, *6*, 10902–10909. [[CrossRef](#)]
15. Fan, B.; Zhang, K.; Jiang, X.F.; Ying, L.; Huang, F.; Cao, Y. High-Performance Nonfullerene Polymer Solar Cells based on Imide-Functionalized Wide-Bandgap Polymers. *Adv. Mater.* **2017**, *29*, 1606396. [[CrossRef](#)]
16. Jessop, I.A.; Bustos, M.; Hidalgo, D.; Terraza, C.A.; Tundidor-Camba, A.; Pardo, M.A.; Fuentealba, D.; Hssein, M.; Bernede, J.C. Synthesis of 2H-benzotriazole based donor-acceptor polymers bearing carbazole derivative as pendant groups: Optical, electrical and photovoltaic properties. *Int. J. Electrochem. Sci.* **2016**, *11*, 9822–9838. [[CrossRef](#)]
17. Yuan, J.T.; Hou, J.J.; Liu, X.L.; Feng, Y.R.; Zhang, X.M. Optimized trimetallic benzotriazole-5-carboxylate MOFs with coordinately unsaturated active sites as an efficient electrocatalyst for the oxygen evolution reaction. *Dalton Trans.* **2020**, *49*, 750–756. [[CrossRef](#)]
18. Kuznetsov, Y.I. Triazoles as a class of multifunctional corrosion inhibitors. A review. Part, I. 1,2,3-Benzotriazole and its derivatives. Copper, zinc and their alloys. *Int. J. Corros. Scale Inhib.* **2018**, *7*, 271–307.
19. Briguglio, I.; Piras, S.; Corona, P.; Gavini, E.; Nieddu, M.; Boatto, G.; Carta, A. Benzotriazole: An overview on its versatile biological behavior. *Eur. J. Med. Chem.* **2015**, *97*, 612–648. [[CrossRef](#)]
20. Carta, A.; Loriga, G.; Piras, S.; Paglietti, G.; Ferrone, M.; Fermeglia, M.; Pricl, S.; La Colla, P.; Secci, B.; Collu, G.; et al. Synthesis and in vitro evaluation of the anti-viral activity of N-[4-(1H(2H) benzotriazol-1(2)-yl)phenyl]alkylcarboxamides. *Med. Chem.* **2006**, *2*, 577–589. [[CrossRef](#)]
21. Carta, A.; Briguglio, I.; Piras, S.; Corona, P.; Boatto, G.; Nieddu, M.; Giunchedi, P.; Marongiu, M.E.; Giliberti, G.; Iuliano, F.; et al. Quinoline tricyclic derivatives. Design, synthesis and evaluation of the antiviral activity of three new classes of RNA-dependent RNA polymerase inhibitors. *Bioorg. Med. Chem.* **2011**, *19*, 7070–7084. [[CrossRef](#)]
22. Yan, R.; Gargas, D.; Yang, P. Nanowire Photonics. *Nat. Photon.* **2009**, *3*, 569–576. [[CrossRef](#)]
23. Yan, Y.; Zhao, Y.S. Organic nanophotonics: From controllable assembly of functional molecules to low-dimensional materials with desired photonic properties. *Chem. Soc. Rev.* **2014**, *43*, 4325–4340. [[CrossRef](#)]
24. Hunsperger, R.G. *Integrated Optics: Theory and Technology*; Springer: Berlin, Germany, 2002.
25. Lal, S.; Link, S.; Halas, N.J. Nano-optics from sensing to waveguiding. *Nat. Photon.* **2007**, *1*, 641–648. [[CrossRef](#)]
26. Clark, J.; Lanzani, G. Organic photonics for communications. *Nat. Photon.* **2010**, *4*, 438–446. [[CrossRef](#)]
27. Cáceres, D.; Cebrián, C.; Rodríguez, A.R.; Carrillo, J.R.; Díaz-Ortiz, A.; Prieto, P.; Aparicio, F.; García, F.; Sánchez, L. Optical waveguides from 4-aryl-4H-1,2,4-triazole-based supramolecular structures. *Chem. Commun.* **2013**, *49*, 621–623. [[CrossRef](#)]
28. Pastor, M.J.; Torres, I.; Cebrián, C.; Carrillo, J.R.; Díaz-Ortiz, A.; Matesanz, E.; Buendía, J.; García, F.; Barberá, J.; Prieto, P.; et al. 4-Aryl-3,5-bis(arylethynyl)aryl-4H-1,2,4-triazoles: Multitasking Skeleton as a Self-Assembling Unit. *Chem. Eur. J.* **2015**, *21*, 1795–1802. [[CrossRef](#)] [[PubMed](#)]
29. Wettach, H.; Pasker, F.; Höger, S. 2-Aryl-2H-benzotriazoles as Building Blocks for New Low-Bandgap Poly(arylene–ethynylene)s. *Macromolecules* **2008**, *41*, 9513–9515. [[CrossRef](#)]
30. Torres, I.; Carrillo, J.R.; Díaz-Ortiz, A.; Martín, R.; Gómez, M.V.; Stegemann, L.; Strassert, C.A.; Orduna, J.; Buendía, J.; Greciano, E.E.; et al. Self-assembly of T-shape 2H-benzo[d][1,2,3]-triazoles. Optical waveguide and photophysical properties. *RSC Adv.* **2016**, *6*, 36544–36553. [[CrossRef](#)]
31. Meier, H. Conjugated Oligomers with Terminal Donor–Acceptor Substitution. *Angew. Chem. Int. Ed.* **2005**, *44*, 2482–2506. [[CrossRef](#)]
32. Mulliken, R.S.; Person, W.B. Donor-Acceptor Complexes. *Annu. Rev. Phys. Chem.* **1962**, *13*, 107–126. [[CrossRef](#)]
33. Foster, R. *Organic Charge-Transfer Complexes*; Academic Press: New York, NY, USA, 1969.
34. Foster, R. Electron donor-acceptor complexes. *J. Phys. Chem.* **1980**, *84*, 2135–2141. [[CrossRef](#)]
35. Wang, J.L.; Xiao, Q.; Pei, J. Benzothiadiazole-Based D– $\pi$ -A– $\pi$ -D Organic Dyes with Tunable Band Gap: Synthesis and Photophysical Properties. *J. Org. Lett.* **2010**, *12*, 4164–4167. [[CrossRef](#)] [[PubMed](#)]
36. Homnick, P.J.; Tinkham, J.S.; Devaughn, R.; Lahti, P.M. Engineering Frontier Energy Levels in Donor–Acceptor Fluoren-9-ylidene Malononitriles versus Fluorenones. *J. Phys. Chem. A* **2014**, *118*, 475–486. [[CrossRef](#)]
37. Lu, X.; Fan, S.; Wu, J.; Jia, X.; Wang, Z.S.; Zhou, G. Controlling the Charge Transfer in D–A–D Chromophores Based on Pyrazine Derivatives. *J. Org. Chem.* **2014**, *79*, 6480–6489. [[CrossRef](#)] [[PubMed](#)]
38. Turro, N.J.; Ramamurthy, V.; Scaianon, J.C. *Modern Molecular Photochemistry of Organic Molecules*; University Science Books: Sausalito, CA, USA, 2010.
39. Turro, N.J.; Ramamurthy, V.; Scaiano, J.C. *Modern Molecular Photochemistry of Organic Molecules*. *Photochem. Photobiol.* **2012**, *88*, 1033. [[CrossRef](#)]
40. Varughese, S. Non-covalent routes to tune the optical properties of molecular materials. *J. Mater. Chem. C* **2014**, *2*, 3499–3516. [[CrossRef](#)]
41. Wang, X.A.; Zhou, Y.; Lei, T.; Hu, N.; Chen, E.Q.; Pei, J. Structural–Property Relationship in Pyrazino[2,3-g]quinoxaline Derivatives: Morphology, Photophysical, and Waveguide Properties. *Chem. Mater.* **2010**, *22*, 3735–3745. [[CrossRef](#)]
42. Ando, S.; Murakami, R.; Nishida, J.I.; Tada, H.; Inoue, Y.; Tokito, S.; Yamashita, Y. n-Type Organic Field-Effect Transistors with Very High Electron Mobility Based on Thiazole Oligomers with Trifluoromethylphenyl Groups. *J. Am. Chem. Soc.* **2005**, *127*, 14996–14997. [[CrossRef](#)]

43. Deng, P.; Yan, Y.; Wang, S.D.; Zhang, Q. Naphthoylene(trifluoromethylbenzimidazole)-dicarboxylic acid imides for high-performance n-type organic field-effect transistors. *Chem. Commun.* **2012**, *48*, 2591–2593. [[CrossRef](#)]
44. Sonar, P.; Ng, G.M.; Lin, T.T.; Dodabalapur, A.; Chen, Z.K. Solution processable low bandgap diketopyrrolopyrrole (DPP) based derivatives: Novel acceptors for organic solar cells. *J. Mater. Chem.* **2010**, *20*, 3626–3636. [[CrossRef](#)]
45. Chung, J.W.; Youç, Y.; Huh, H.S.; An, B.K.; Yoon, S.J.; Kim, S.H.; Lee, S.W.; Park, S.Y. Shear- and UV-Induced Fluorescence Switching in Stilbenic  $\pi$ -Dimer Crystals Powered by Reversible [2 + 2] Cycloaddition. *J. Am. Chem. Soc.* **2009**, *131*, 8163–8172. [[CrossRef](#)] [[PubMed](#)]
46. Torres, I.; Díaz-Ortiz, A.; Sánchez, L.; Orduña, J.; Blesa, M.J.; Carrillo, J.R.; Prieto, P. Tunable emission in aggregated T-Shaped 2H-Benzo[d][1,2,3]triazoles with waveguide behaviour. *Dyes Pigm.* **2017**, *142*, 212–225. [[CrossRef](#)]
47. Grigorenko, A.N.; Polini, M.; Novoselov, K.S. Graphene plasmonics. *Nat. Photon.* **2012**, *6*, 749–758. [[CrossRef](#)]
48. Novoselov, K.S.; Geim, A.K.; Morozov, S.V.; Jiang, D.; Zhang, Y.; Dubonos, S.V.; Grigorieva, I.V.; Firsov, A.A. Electric Field Effect in Atomically Thin Carbon Films. *Science* **2004**, *306*, 666–669. [[CrossRef](#)]
49. Mueller, T.; Xia, F.; Avouris, P. Graphene photodetectors for high-speed optical communications. *AC Nat. Photon.* **2010**, *4*, 297–301. [[CrossRef](#)]
50. Wi, D.; Tian, J.; Li, L.; Yang, R. Plasmon induced transparency and refractive index sensing in a new type of graphene-based plasmonic waveguide. *Opt. Commun.* **2018**, *412*, 41–48.
51. Liuc, M.; Yin, X.; Zhang, X. Double-Layer Graphene Optical Modulator. *Nano Lett.* **2012**, *12*, 1482–1485.
52. Koester, S.J.; Li, M. High-speed waveguide-coupled graphene-on-graphene optical modulators. *Appl. Phys. Lett.* **2012**, *100*, 171107. [[CrossRef](#)]
53. León, V.; Quintana, M.; Herrero, M.A.; Fierro, J.L.G.; de la Hoz, A.; Prato, M.; Vázquez, E. Few-layer graphenes from ball-milling of graphite with melamine. *Chem. Commun.* **2011**, *47*, 10936–10938. [[CrossRef](#)]
54. León, V.; Rodríguez, A.M.; Prieto, P.; Prato, M.; Vazquez, E. Exfoliation of Graphite with Triazine Derivatives under Ball-Milling Conditions: Preparation of Few-Layer Graphene via Selective Noncovalent Interactions. *ACS Nano* **2014**, *8*, 563–571. [[CrossRef](#)]
55. Gonzalez-Domínguez, J.M.; León, V.; Lucío, M.I.; Prato, M.; Vázquez, E. Production of ready-to-use few-layer graphene in aqueous suspensions. *Nat. Protoc.* **2018**, *13*, 495–506. [[CrossRef](#)]
56. Torres, I.; Gonzalez-Domínguez, J.M.; Díaz-Ortiz, A.; Romero-Nieto, C.; Rominguer, F.; Vázquez, E.; Carrillo, J.R.; Prieto, P. Modulation of waveguide behaviour of an ICT 2H-Benzo[d][1,2,3]Triazole derivative with graphene. *Org. Electron.* **2019**, *68*, 1–8. [[CrossRef](#)]
57. Wakayama, Y.; Hayakawa, R.; Seo, H.-S. Recent progress in photoactive organic field-effect transistors. *Sci. Technol. Adv. Mater.* **2014**, *15*, 024202. [[CrossRef](#)]
58. Torsi, L.; Magliulo, M.; Manoli, K.; Palazzo, G. Organic field-effect transistor sensors: A tutorial review. *Chem. Soc. Rev.* **2013**, *42*, 8612–8628. [[CrossRef](#)] [[PubMed](#)]
59. Size, S.M.; Lee, M.K. *Semiconductor Devices: Physics and Technology*, 3rd ed.; Wiley: New York, NY, USA, 2012.
60. Ponce, R.; Facchetti, A.; Marks, T.J. High-k Organic, Inorganic, and Hybrid Dielectrics for Low-Voltage Organic Field-Effect Transistors. *Chem. Rev.* **2010**, *110*, 205–239.
61. Torres-Moya, I.; Arrechea-Marcos, I.; Tardío, C.; Carrillo, J.R.; Díaz-Ortiz, A.; López Navarrete, J.T.; Ruiz Delgado, M.C.; Prieto, P.; Ponce, R. D–A–D 2H-benzo[d][1,2,3]triazole derivatives as p-type semiconductors in organic field-effect transistors. *RSC Adv.* **2018**, *8*, 21879–21888. [[CrossRef](#)]
62. Strickler, J.H.; Webb, W.W. *CAN-AM Easten '90*; Antos, R.L., Krisiloff, A.J., Eds.; International Society for Optics and Photonics: Bellingham, WA, USA, 2012; pp. 107–118.
63. Strickler, J.H.; Webb, W.W. Three-dimensional optical data storage in refractive media by two-photon point excitation. *Opt. Lett.* **1991**, *16*, 1780–1782.
64. Denk, W.; Strickler, J.H.; Webb, W.W. Two-photon laser scanning fluorescence microscopy. *Science* **1990**, *248*, 73–76. [[CrossRef](#)] [[PubMed](#)]
65. Mongin, O.; Porrès, L.; Charlot, M.; Katan, C.; Blanchard-Desce, M. Synthesis, Fluorescence, and Two-Photon Absorption of a Series of Elongated Rodlike and Banana-Shaped Quadrupolar Fluorophores: A Comprehensive Study of Structure–Property Relationships. *Chem. Eur. J.* **2007**, *13*, 1481–1498. [[CrossRef](#)]
66. Chung, S.J.; Zheng, S.; Odani, T.; Beverina, L.; Fu, J.; Padilha, L.A.; Biesso, A.; Hales, J.M.; Zhan, X.; Schmidt, K.; et al. Extended Squaraine Dyes with Large Two-Photon Absorption Cross-Sections. *J. Am. Chem. Soc.* **2006**, *128*, 14444–14445. [[CrossRef](#)]
67. Albota, M.; Hess, S.E.; Webb, W.W.; Xu, C.; Beljonne, D.; Brédas, J.; Fu, J.Y.; Heikal, A.A.; Rumi, M.; Wu, X.L.; et al. Design of Organic Molecules with Large Two-Photon Absorption Cross Sections. *Science* **1998**, *281*, 1653–1656. [[CrossRef](#)] [[PubMed](#)]
68. Beverina, L.; Fu, J.; Leclercq, A.; Zojer, E.; Pacher, P.; Barlow, S.; Van Stryland, E.W.; Hagan, D.J.; Brédas, J.L.; Marder, S.R. Two-Photon Absorption at Telecommunications Wavelengths in a Dipolar Chromophore with a Pyrrole Auxiliary Donor and Thiazole Auxiliary Acceptor. *J. Am. Chem. Soc.* **2005**, *127*, 7282–7283. [[CrossRef](#)] [[PubMed](#)]
69. Varnavski, O.; Yan, X.; Mongin, O.; Blanchard-Desce, M.; Goodson, T. Strongly Interacting Organic Conjugated Dendrimers with Enhanced Two-Photon Absorption. *J. Phys. Chem. C* **2007**, *111*, 149–162. [[CrossRef](#)]
70. Pawlicki, M.; Collins, H.A.; Denning, R.G.; Anderson, H.L. Two-photon absorption and the design of two-photon dyes. *Angew. Chem. Int. Ed. Engl.* **2009**, *48*, 3244–3266. [[CrossRef](#)] [[PubMed](#)]

71. Kato, S.I.; Matsumoto, T.; Ishi-I, T.; Thiemann, T.; Shigeiwa, M.; Gorohmaru, H.; Maeda, S.; Yamashita, Y.; Mataka, S. Strongly red-fluorescent novel donor- $\pi$ -bridge-acceptor- $\pi$ -bridge-donor (D- $\pi$ -A- $\pi$ -D) type 2,1,3-benzothiadiazoles with enhanced two-photon absorption cross-sections. *Chem. Commun.* **2004**, *10*, 2342–2343. [[CrossRef](#)]
72. Kato, S.I.; Matsumoto, T.; Shigeiwa, M.; Gorohmaru, H.; Maeda, S.; Ishi-i, T.; Mataka, S. Novel 2,1,3-Benzothiadiazole-Based Red-Fluorescent Dyes with Enhanced Two-Photon Absorption Cross-Sections. *Chem. Eur. J.* **2006**, *12*, 2303–2317. [[CrossRef](#)]
73. Yang, Z.D.; Feng, J.K.; Ren, A.M. Theoretical study of one-photon and two-photon absorption properties for 2,1,3-benzothiadiazole-based red-fluorescent dyes. *J. Mol. Struct. Theochem* **2008**, *848*, 24–33. [[CrossRef](#)]
74. Martín, R.; Prieto, P.; Carrillo, J.R.; Torres, I.; Strassert, C.A.; Soloviova, K.; Rodríguez, M.A.; Sánchez, L.; Díaz-Ortiz, A. Colored optical waveguides in self-assembled thiadiazole-based materials. *Dyes Pigm.* **2018**, *151*, 327–334. [[CrossRef](#)]
75. Martín, R.; Prieto, P.; Carrillo, J.R.; Rodríguez, A.M.; de Cózar Boj, A.P.G.; Díaz-García, M.A.; Ramírez, M.G. Design, synthesis and amplified spontaneous emission of 1,2,5-benzothiadiazole derivatives. *J. Mater. Chem. C* **2019**, *7*, 9996–10007. [[CrossRef](#)]
76. Torres-Moya, I.; Benitez-Martín, C.; Donoso, B.; Tardio, C.; Martín, R.; Carrillo, J.R.; Díaz-Ortiz, A.; Nájera, F.; Prieto, P.; Pérez-Inestrosa, E. Extended Alkenyl and Alkynyl Benzotriazoles with Enhanced Two-Photon Absorption Properties as a Promising Alternative to Benzothiadiazoles. *Chem. Eur. J.* **2019**, *25*, 15572–15579. [[CrossRef](#)]
77. Moniruzzaman, M.; Sundarajan, P.R. Low molecular weight organogels based on long-chain carbamates. *Langmuir* **2005**, *21*, 3802–3807. [[CrossRef](#)]
78. Rao, M.R.; Sun, S. Supramolecular Assemblies of Amide-Derived Organogels Featuring Rigid  $\pi$ -Conjugated Phenylethynyl Frameworks. *Langmuir* **2013**, *29*, 15146–15158. [[CrossRef](#)]
79. Dou, C.D.; Chem, D.; Iqbal, J.; Yuan, Y.; Zhang, H.Y. Multistimuli-Responsive Benzothiadiazole-Cored Phenylene Vinylene derivative with nanoassembly properties. *Langmuir* **2011**, *27*, 6323–6329. [[CrossRef](#)] [[PubMed](#)]
80. Chung, J.W.; Yoon, S.-J.; Lim, S.-J.; An, B.-K.; Park, S.Y. Dual-Mode Switching in Highly Fluorescent Organogels: Binary Logic Gates with Optical/Thermal Inputs. *Angew. Chem. Int. Ed.* **2009**, *48*, 7030–7034. [[CrossRef](#)]
81. Prathap, A.; Sureshan, K.M. A mannitol based phase selective supergelator offers a simple, viable and greener method to combat marine oil spills. *Chem. Commun.* **2012**, *48*, 5250–5252. [[CrossRef](#)] [[PubMed](#)]
82. Wezenberg, S.J.; Croisetu, C.M.; Stuart, M.C.A.; Feringa, B.L. Reversible gel-sol photoswitching with an overcrowded alkene-based bis-urea supergelator. *Chem. Sci.* **2016**, *7*, 4341–4346. [[CrossRef](#)]
83. Van Gorp, J.J.; Vekemans, J.A.J.N.; Meijer, E.W. C3-Symmetrical Supramolecular Architectures: Fibers and Organic Gels from Discotic Trisamides and Trisureas. *J. Am. Chem. Soc.* **2002**, *124*, 14759–14769. [[CrossRef](#)] [[PubMed](#)]
84. Ya Malkin, A.; Isayev, A.I. *Rheology: Concepts, Methods and Applications*, 3rd ed. Chemtech Publishing: Toronto, ON, Canada, 2016.
85. Matsuo, K.; Matsuoka, M. Solid-State Polymorphic Transition of Theophylline Anhydrate and Humidity Effect. *Cryst. Growth Des.* **2007**, *7*, 411–415. [[CrossRef](#)]
86. Seton, L.; Khamar, D.; Bradshaw, I.J.; Hutcheon, G.A. Solid State Forms of Theophylline: Presenting a New Anhydrous Polymorph. *Cryst. Growth Des.* **2010**, *10*, 3879–3886. [[CrossRef](#)]
87. Patel, M.K.; Tailor, S.M.; Patel, U.H. DFT study and Hirshfeld surface analysis of third polymorph of sulfamerazine. *AIP Conf. Proc.* **2016**, *1728*, 020257.
88. Munroe, A.; Rasmuson, A.C.; Modnett, B.K.; Croker, D.M. Relative Stabilities of the Five Polymorphs of Sulfathiazole. *Cryst. Growth Des.* **2012**, *12*, 2825–2835. [[CrossRef](#)]
89. Anwar, J.; Tarling, S.E.; Barnes, P. Polymorphism of Sulfathiazole. *J. Pharm. Sci.* **1989**, *78*, 337–342. [[CrossRef](#)]
90. Torres-Moya, I.; Saikia, B.; Prieto, P.; Carrillo, J.R.; Steed, B.J.W. High thermal stability, pH responsive organogels of 2H-benzotriazole derivatives as pharmaceutical crystallization media. *Cryst. Eng. Comm.* **2019**, *21*, 2135–2142. [[CrossRef](#)]
91. Wolfbeis, O.S. An overview of nanoparticles commonly used in fluorescent bioimaging. *Chem. Soc. Rev.* **2015**, *44*, 4743–4768. [[CrossRef](#)] [[PubMed](#)]
92. Kolemen, S.; Akkaya, E.U. Reaction-based BODIPY probes for selective bio-imaging. *Coord. Chem. Rev.* **2018**, *354*, 121–134. [[CrossRef](#)]
93. Chen, F.; Gerion, D. Fluorescent CdSe/ZnS nanocrystal-peptide conjugates for long-term, nontoxic imaging and nuclear targeting in living cells. *Nano. Lett.* **2004**, *4*, 1827–1832. [[CrossRef](#)]
94. Zhan, R.; Liu, B. Benzothiadiazole-containing conjugated polyelectrolytes for biological sensing and imaging. *Macromol. Chem. Phys.* **2015**, *216*, 131–144. [[CrossRef](#)]
95. Dias, F.B.; King, S.; Monkman, A.P.; Perepichka, I.I.; Kryuchkov, M.A.; Perepichka, I.F.; Bryce, M.R. Dipolar stabilization of emissive singlet charge transfer excited states in polyfluorene copolymers. *J. Phys. Chem. B* **2008**, *112*, 6557–6566. [[CrossRef](#)] [[PubMed](#)]
96. Shi, H.; Sun, H.; Yang, H.; Liu, S.; Jenkins, G.; Feng, W.; Li, F.; Zhao, Q.; Liu, B.; Huang, W. Cationic polyfluorenes with phosphorescent iridium(III) complexes for time-resolved luminescent biosensing and fluorescence lifetime imaging. *Adv. Funct. Mater.* **2013**, *23*, 3268–3276. [[CrossRef](#)]
97. Liu, B.; Bazan, G.C. Synthesis of cationic conjugated polymers for use in label-free DNA microarrays. *Nat. Protoc.* **2006**, *1*, 1698–1702. [[CrossRef](#)] [[PubMed](#)]
98. Mallavia, R.; Martinez-Peréz, D.; Chmelka, B.F.; Bazan, G.C. Blue fluorescent films based on poly-2,7-fluorene-phenylene derivatives. *Bol. Soc. Esp. Ceram. Vidr.* **2004**, *43*, 327–330. [[CrossRef](#)]

99. Molina, R.; Gómez-Ruiz, S.; Montilla, F.; Salinas-Castillo, A.; Fernández-Arroyo, S.; Del Mar Ramos, M.; Micol, V.; Mallavia, R. Progress in the synthesis of poly(2,7-fluorene-alt-1,4-phenylene), PFP, via suzuki coupling. *Macromolecules* **2009**, *42*, 5471–5477. [[CrossRef](#)]
100. Kahveci, Z.; Vázquez-Guilló, R.; Martínez-Tomé, M.J.; Mallavia, R.; Mateo, C.R. New Red-Emitting Conjugated Polyelectrolyte: Stabilization by Interaction with Biomolecules and Potential Use as Drug Carriers and Bioimaging Probes. *ACS Appl. Mater. Interfaces* **2016**, *8*, 1958–1969. [[CrossRef](#)]
101. Mira, A.; Mateo, C.R.; Mallavia, R.; Falco, A. Poly(methyl vinyl ether-alt-maleic acid) and ethyl monoester as building polymers for drug-loadable electrospun nanofibers. *Sci. Rep.* **2017**, *7*, 17205. [[CrossRef](#)] [[PubMed](#)]
102. Vázquez, R.; Martínez-Tomé, M.J.; Kahveci, Z.; Torres-Moya, I.; Falco, A.; Mallavia, R.; Reyes, C. Synthesis and Characterization of a Novel Green Cationic Polyfluorene and Its Potential Use as a Fluorescent Membrane Probe. *Polymers* **2018**, *10*, 938. [[CrossRef](#)] [[PubMed](#)]